

Full paper

Battery-free neuromodulator for peripheral nerve direct stimulation

Sanghoon Lee^{a,b,c,d,f,1}, Hao Wang^{a,c,d,f,1}, Jiahui Wang^{a,b,f}, Qiongfeng Shi^{a,c,d,f}, Shih-Cheng Yen^{a,b}, Nitish V. Thakor^{a,b,e,f}, Chengkuo Lee^{a,b,c,d,e,f,*}

^a Department of Electrical and Computer Engineering, National University of Singapore, 4 Engineering 3, Singapore 117583, Singapore

^b Singapore Institute for Neurotechnology (SINAPSE), National University of Singapore, Singapore 117456, Singapore

^c Center for Intelligent Sensors and MEMS, National University of Singapore, 4 Engineering Drive 3, Singapore 117576, Singapore

^d NUS Suzhou Research Institute (NUSRI), Suzhou, Industrial Park, Suzhou 215123, PR China

^e Graduate School for Integrative Science and Engineering, National University of Singapore, Singapore 117456, Singapore

^f Hybrid Integrated Flexible Electronic Systems (HiFES), National University of Singapore, 5 Engineering Drive 1, Singapore 117608, Singapore

ARTICLE INFO

Keywords:

Batter-free
Neuromodulator
Peripheral nerve
Direct stimulation
Neuroprosthesis
Neural interface

ABSTRACT

Modulation of peripheral nerves is an emerging field for neuroprosthesis and bioelectronic medicine. With developing neural interfacing technology (NIT) that directly communicates with peripheral nerves, several powering schemes have been investigated for long-term use of implantable devices such as wireless and conversion of human body energy. Recently, a variety of promising energy harvesters have been demonstrated as alternatives to solve the power supply issue. Triboelectric nanogenerators (TEGs) show promising performance as a power source of a neuro-stimulator since the output of TENGs provides direction stimulation of a nerve. However, there is a lack of research on TENGs for peripheral nerve stimulation.

This work introduces a novel water/air-hybrid triboelectric nanogenerator (WATENG) to overcome current drawbacks of liquid based TENGs as well as to achieve efficient nerve stimulation. Furthermore, this study involves comparative demonstration of the efficiency of nerve stimulation induced by exponential and square pulsed waveforms, to verify that TENGs can effectively stimulate nerves and are good candidates for neurostimulators. By combining this device with neural interfaces, selective and force-controlled modulation of leg muscles in rats can be achieved.

1. Introduction

Modulation of neural signals using implantable bioelectronics, which includes neuroprosthesis for restoration of sensory/motor function [1–3] and bioelectronic medicine for modulation of peripheral visceral nerves to control the bodily functions or treat diseases [4–6], are intensively investigated as a promising research field toward the next generation of neurotechnology. Achieving lasting effect of the modulation requires long-term use of an implantable neurostimulator that allows the energy-efficient neuro-stimulation inside the human body. Especially for achieving the modulation of muscles or organs via the nervous system, two main components of a neurostimulator should be considered: a stimulator and a neural interface. For the neural interface, selectivity of stimulation is carefully considered with invasiveness when to design a peripheral neural interface. Ideally, peripheral neural interfaces should show the highest selectivity with the minimum invasiveness. However, due to the anatomical limitation of peripheral nerves, selectiveness and invasiveness are always trade-off.

Intrafascicular approaches enhance the selectivity but, compromise the invasiveness [7]. Previous studies demonstrated that close contact with unique designs and flexible materials allowed to enhance the selectivity of recording and stimulation via extraneural approaches [8–13]. Furthermore, approaching small branches of a nerve enabled to enhance functional selectivity and to eliminate the effort of enhancing selectivity such as the large number of electrode contacts and topographical positions of electrodes contacts in case of sciatic nerves [9,12].

For the stimulator, square-wave pulses are typically used as an input signal [14]. While some studies also reported that exponential waveforms can realize a more effective neuron stimulation with lower power consumption than that by square-wave pulse [15,16]. However, there are few studies on device development for generating exponential waveforms compared with ones for square-wave pulses, as well as on relevant to *in vivo* experiments. Therefore, the development of novel devices, which enables generating exponential waveforms and implantation for long-term use, are highly required.

The self-powered concept for biomedical devices has been explored

* Corresponding author at: Department of Electrical and Computer Engineering, National University of Singapore, 4 Engineering 3, Singapore 117583, Singapore.

¹ Both authors contributed equally.

using various mechanisms, which is recently attracting significant attention as a novel self-sustainable platform for long-term use [17–21]. Triboelectric nanogenerators (TENGs) are a promising technology in that it scavenges human body energy into useful electrical power using the detection of various mechanical sources [22–30]. It is also applicable for chronic implantation using bio-materials, which may allow to realize implantable platforms of TENGs with neural interfaces in the future [31,32]. More importantly, TENGs generate exponential current waveforms as an output signal which can be used for direct neuro-stimulation as a power source [12,33]. Although both current amplitude and charge amount of the TENGs output were all lower than the threshold level required for neuron stimulation by square wave current, our previous study showed clear muscle activations with TENGs by stimulating a sciatic nerve and branches [12]. Since lower charges reduce the risk of stimulation induced tissue and electrode damages, neuro-stimulation by TENGs has promising potentials to be used as a novel stimulation source. Compared with the stack-layer design in our previous study [12], the liquid based TENG involved in this study can achieve an equal or even better performance but with a smaller pixel area [34–38], enabling a multi-pixel device to achieve multi-selective stimulations.

2. System and device configuration, and *in vivo* demonstration

Demonstration of applicable designs for practical uses and a profound understanding of efficient neuro-stimulation by TENGs is highly required to move to the next phase of clinical applications, which may open up a new era of direction stimulation for neuroprosthesis or bioelectronics medicine. Here, we propose a new liquid based TENG array device where each neural electrode is connected with an individual pixel on the device, which provides multiple and selective stimulations (Fig. 1). This concept of the device may provide functional electrical stimulation (FES) or rehabilitation solutions (Fig. 1c,d). We developed sponge involved water/air-hybrid triboelectric

nanogenerator (WATENG) with single pixel to fully overcome all these drawbacks, such as liquid evaporation issue, lack of liquid fixation mechanism and low output, as well as to be used as a stimulator. An array based WATENG device with involvement of sponge and suspended dielectric thin film is proposed (Fig. 1a).

Hydrogel suggested an alternative to water droplets to improve the evaporation and fixation issues [39,40], however, the shape of the hydrogel bead irreversibly collapse by dehydration and cannot fully recover even when soaked in water. Furthermore, the hydrogel is fragile and tends to break when a large pressing force is applied, so that the actual working range of force sensing is limited. Compared with hydrogel, the sponge implemented here can fix the position of water. Besides, the change of contact area provided by sponge filled with water is not limited by the top surface area of the sponge. Since water can be squeezed out of the sponge, output higher than hydrogel based device of the same area can be achieved with sponge devices. Although the evaporation is still inevitable, water can be refilled into the sponge without affecting the performance, making the device more reliable. The suspended dielectric thin film above the sponge will have negative electrostatic charge induction on both sides during the cycle of pressing, which can significantly amplify the output. This amplified output is capable for direct stimulation of a peripheral nerve.

The WATENG is demonstrated as a battery-free neuromodulator for peripheral nerve stimulation by various *in vivo* experiments using a variety of neural interfaces. Firstly, to demonstrate selective modulation of peripheral nerves using WATENG arrays (Fig. 1b and c), we conducted selective stimulation of a sciatic nerve in rats using flexible sling interfaces. Secondly, to demonstrate a force-controlled modulation, we stimulated branches of sciatic nerves using Pt/Ir wires. In this experiment, very high efficient stimulation was observed, which cannot be well explained by the well known charge-based nerve stimulation theory. Therefore, we investigated the efficiency of exponential waveforms generated by WATENG compared with square pulsed waveform, which is conventionally used for nerve stimulation, with flexible neural

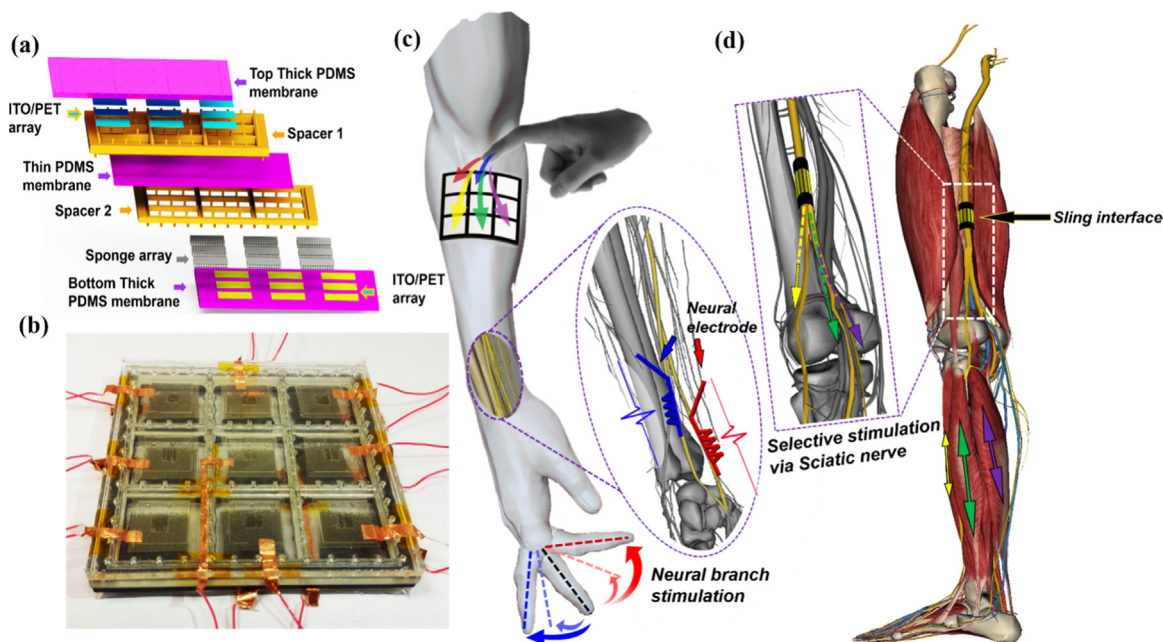


Fig. 1. Conceptual illustration of battery free neuromodulation combining with WATENG and neural electrodes. (a) Illustration of layer structure of the WATENG; (b) Optical image of the prototype of the WATENG. (c) Illustration of direct neural branch stimulation by WATENG via neural electrodes wrapped around neural branches. The nerve branches wrapped by red and blue neural electrodes can be stimulated by the pixels pointed by red and blue arrows, respectively. Each nerve branch will control one muscle, thus a finger can bend or straight just by pressing the red or blue pixel. (d) Illustration of selective stimulation of a sciatic nerve by WATENG signals via a flexible sling interface wrapped around the sciatic nerve. The three nerve trunks within the sciatic nerve, indicated by the yellow, green and purple arrows, can be stimulated by different groups of electrodes surrounding the sling interface. And each group of electrodes can be activated by the pixels pointed by the yellow, green and purple arrows, respectively. Each nerve trunk controls one muscle on leg. By pressing different pixels, different muscles will be activated to induce either plantar flexion or ankle dorsiflexion.

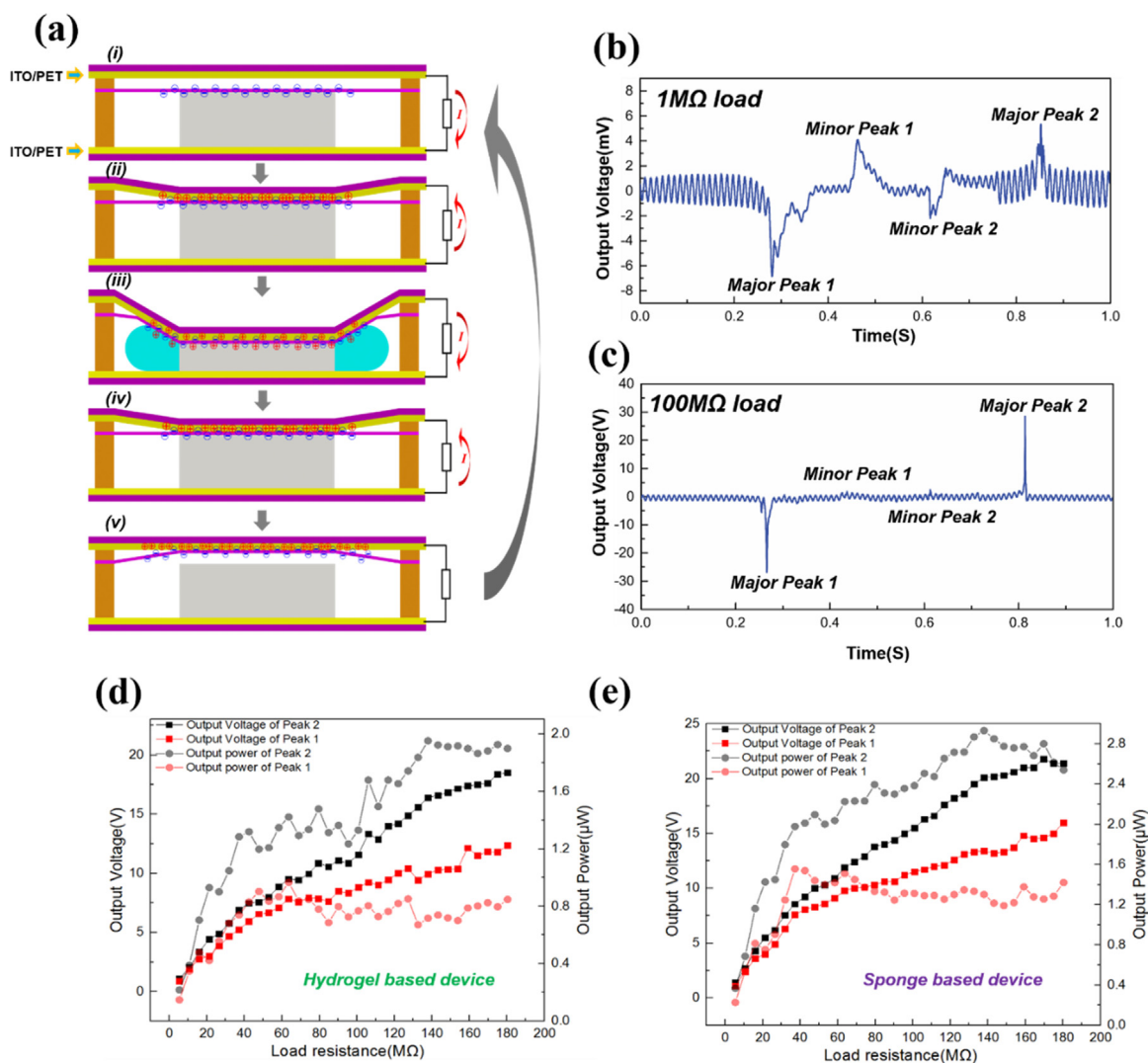


Fig. 2. Characterization of the WATENG. (a) Working principle of the WATENG; Voltage output of the whole operation cycle in (b) when 1 MΩ load is applied and in (c) when 100 MΩ load is applied. (d) The output voltage and output power for major peaks of the device with hydrogel with different load resistance. (e) The output voltage and output power for major peaks of device with sponge with different load resistance.

clip (FNS) interfaces. With this comparison, we confirmed that an exponential wave could achieve higher nerve stimulation efficiency than the square pulse wave. Therefore, with the array of WATENG where each pixel is connected with either neural electrodes wrapped on different peripheral nerves or different electrode groups on a sling interface wrapped around the sciatic nerve (Fig. 1c and d), a controllable neurostimulator for multiple muscle modulations can be realized by tapping different pixels with different forces.

3. Working mechanism

The layer structure of the array device for WATENG is shown in Fig. 2a and the optical image of the prototype is shown in Fig. 2b. The top and bottom 2-mm-thick PDMS membranes with ITO-coated PET array acted as the two electrodes required for TENGs. Between these two thick PDMS membranes, a thin PDMS membrane of 20 μm thickness was clamped by two spacers made by 3D printing. A sponge array filled with water was arranged within the grid array of the Spacer 2. The dimension for each grid and sponge was 2 cm × 2 cm and 1.5 cm × 1.5 cm, respectively. The thickness of the sponge was 2 mm, which is the same as the thickness of the Spacer 2. A detailed fabrication and assembly process is illustrated in the [Supplementary information S1](#).

The working principle of WATENG is illustrated in Fig. 2a. After the operation of the first cycle, the top and bottom surfaces of the suspended PDMS membrane have electrification with the ITO electrode on the top surface and water, which is squeezed out from the sponge, respectively. Hence, both sides of this thin PDMS membrane has negative electrostatic charges upon the surfaces, which is the initial state as shown in Fig. 2a-i. When a pressing force is applied onto the top PDMS membrane, a deformation occurs and induces the contact between the ITO electrode and top surface of the thin PDMS membrane (Fig. 2a-ii). Positive charges are coupled onto the ITO surface to balance the negative charge on both sides of the thin PDMS membrane, inducing a current flow from bottom electrode to top electrode, which is the major peak 1 indicated in Fig. 2b and c. The applied force is increased to press the top PDMS membrane further and squeezes the water out of the sponge beneath the thin PDMS membrane as shown in Fig. 2a-iii. Because of the conductive nature, water contacting with the bottom ITO electrode acts as the extension of bottom electrode. Thus, the negative charges on both sides of the thin PDMS membrane is now coupled by the positive charges on both the top ITO electrode and water surface beneath the thin PDMS membrane. It means a portion of the positive charges initially on the top ITO surface will be transferred to the bottom water surface and induce a backward current flow which is the minor peak 1. After releasing the force, water will be absorbed by the sponge

first (Fig. 2a-iv). Without contact between water and bottom surface of the thin PDMS film, all the negative charges on both sides of the thin PDMS film can only be balanced by the positive charges on the top ITO electrode, thus a current flow from bottom electrode to top electrode is induced, i.e., the minor peak 2. Then the top thick PDMS membrane will further recover to the original position. Due to the sticky surface of the thin PDMS layer, this thin PDMS membrane will be lifted up to some extent (Fig. 2a-v) and then detaches from the top ITO surface (Fig. 2a-i). A backward current will induce the major peak 2. The detailed voltage curves measured with 1 M Ω and 100 M Ω load resistances are shown in Fig. 2b and c. To carefully study each step in the operation, a 0.1 s time interval was set between each step (From Figs. 2a-i to 2a-v) to make all minor and major peaks separate. The amplitude of the 2 major peaks was higher than that of the 2 minor peaks. This is because the charge transferred for major peaks is induced by negative charges on both sides of the thin PDMS layer while the charge transferred for minor peaks is only induced by negative charges on the bottom side. When 1 M Ω load was applied, the minor peaks and major peaks were still comparable. However, when a 100 M Ω load was applied, the major peaks increased from 6 mV to 30 V while the minor peaks were lower than the noise and not detectable. This is because the instantaneous inner impedance for major peaks and minor peaks are different. The triboelectric energy harvester can be simplified as a capacitor with charge generated by electrification. Based on the equation: $Q = C \times U$, when the charge Q is fixed, a higher capacitor C will cause a lower open circuit voltage U .

The minor peaks happen when the top ITO and water all contact with the thin PDMS layer. Thus the inner impedance of this step is mainly determined by the thin PDMS dielectric layer, which is a large capacitor. The major peaks happen when the top ITO contacts and separates from the thin PDMS layer without the contact between water and the thin PDMS layer. The inner impedance of this step is mainly determined by both the thin PDMS layer and the whole space occupied by the sponge, which is a much smaller capacitor. Although the quantity of the charge transferred for minor peaks and major peaks is comparable, due to the huge difference in capacitive impedance, the open circuit voltage of major peaks will be much larger than that of the minor peaks. A detailed analysis can be found in the [Supplementary information S2](#).

One key disadvantage for previous liquid involved TENGs, which have multiple water droplets connecting two plates [35,37,41–43], is that they cannot adapt to different tilt angles. Without a fixation mechanism, water droplets will flow away when the device is not operated on a horizontal plane, which occurs frequently in real applications. In previous research [39,40], hydrogel was considered as an alternative to normal water droplets based TENGs. Hydrogel is a network of polymer chains with superabsorbent capability to water molecules. It is also conductive and can induce the same electrification with water. In general, a hydrogel bead can be considered as a flexible water droplet with specific shape and can be easily immobilized at a certain position. Thus, the sponge based method developed in this study can solve all the issues that hydrogel can. In addition, the sponge based devices provide better performance in three aspects. The first issue is the water evaporation, which will significantly influence the performance of liquid involved TENGs. Although hydrogel can greatly reduce the evaporation and extend the life time of the device, the shape of the hydrogel bead will irreversibly collapse by dehydration and cannot fully recover even when soaked in the water. On the contrary, the shape of the sponge is not affected during the dehydration process and the performance can be fully recovered by refilling with water. Secondly, the sponge is more compressible than hydrogel without the concern of breaking, thus providing a larger force range for sensing applications. Another key point is that sponge based device can generate higher output than hydrogel. This is because the maximum contact area between the hydrogel and dielectric layer cannot exceed its base area [39,40]. But for the sponge, during pressing, the water will not only wet the top surface of the sponge but also be squeezed out of the sponge. Hence the contact

area between water and dielectric layer can exceed the area occupied by the sponge. Given the same area for both hydrogel and sponge, the maximum output of sponge is higher.

A detailed characterization was conducted to prove that the sponge based device can provide a higher output and a larger force sensing range in the same condition. Considering that the hydrogel is less compressible than sponge, to make a fair comparison, same pressing depth, which is 4 mm, was applied in tests instead of same force to avoid hydrogel breakage. The pressing and releasing speed is 900 mm/min. The sponge used in this test is of 2.25 cm² area (1.5 cm \times 1.5 cm square) and the hydrogel is of the same base area (1.7 cm diameter round) but with a hemisphere shape. The detailed structure of the hydrogel based device can be found in the [Supplementary information S3](#).

As emphasized in Fig. 2a, the two major peaks occur when the ITO and PDMS thin film contact and separate at different positions, which is not the situation of conventional TENGs [44–47] when the electrode and dielectric layer contact and separate at the same position. Apparently, the instantaneous inner impedance of the major peak 1 will be smaller than major peak 2. The output voltage and power of two major peaks are characterized individually for a detailed analysis.

Fig. 2d and e show the characterization of the output voltage and output power of the hydrogel-based device and the sponge based device respectively. Generally, the output voltage of peak 1 is lower than that of peak 2. The maximum output power of peak 1 is 0.9 μ W at 47.7 M Ω for the hydrogel based device and 1.56 μ W at 37.1 M Ω for sponge based device. So for peak 1, compared with the hydrogel based device, the sponge based device can achieve higher output with lower inner impedance. This is because peak 1 happens during the pressing process. The contact area between the PDMS thin film and liquid phase (water or hydrogel) for the sponge based device is larger than that of hydrogel. A larger contact area can induce more negative charges on the bottom side of the PDMS thin film, leading to a higher charge transfer, and a lower inner impedance. For peak 2, the sponge based device and the hydrogel based device reach maximum output power of 2.93 μ W and 1.95 μ W, respectively, at the same load 137.8 M Ω . Peak 2 happens when the top ITO surface separates with the PDMS thin film. At this step, the factors determining the inner impedance including the height of air gap, the contact area between ITO and PDMS thin film, are almost identical. Thus, the instantaneous inner impedance is also the same. However, due to the larger contact area between water and the PDMS thin film, more negative charge will be induced at the bottom surface of PDMS thin film and thus will result in a higher output power.

4. Force sensing array

Force-controlled stimulation is also a desirable function for versatile applications of stimulation. One advantage of the exponential wave for nerve stimulation is that the force can have a linear change with the charge quantity. Meanwhile, based on the triboelectric mechanism, this charge quantity is affected by the pressing force. Therefore, a linear control of the charge quantity by force is the key issue to realize a linear stimulation control for muscle activations. To demonstrate the feasibility of force-controlled stimulator, a force sensing capability of the array of WATENG is investigated. Furthermore, when each pixel is connected to different neural electrodes, a force controlled multiple nerve stimulation can be realized. Fig. 3a and b shows the result of force sensing for the hydrogel based and the sponge based device, respectively. Since the minimum force required to make the ITO contact with the PDMS thin film is 14.5 N, all the force curves start when the force is higher than 14.5 N. Meanwhile, the quantity of charges transferred in the whole cycle is also recorded as a reference for direct neural stimulation test because the quantity of the charge is considered as a key factor to induce neural stimulation.

For the hydrogel based device, the voltage and charge increase from 10.5 V to 18.2 V and 9 nC to 16.5 nC, respectively, when the force increases from 14.8 N to 18 N. The higher force will make the voltage and

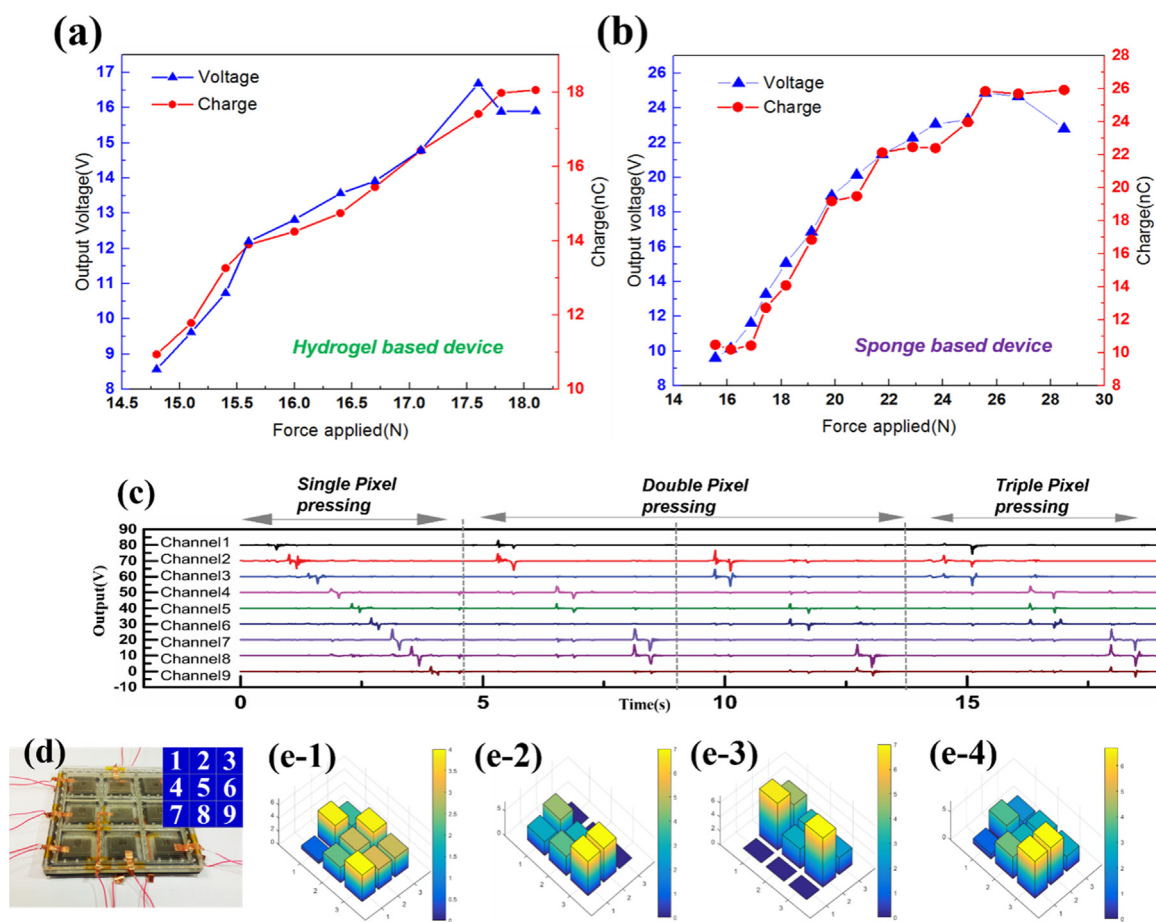


Fig. 3. Force sensing demonstration and characterization. (a) The output voltage and transferred charge of the device with hydrogel with different applied force. (b) The output voltage and transferred charge of the device with sponge with different applied force. (c–e) A sponge based device with 3 by 3 pixel array for force sensing demonstration. (c) Voltage signal of 9 channels for force sensing test by finger pressing. The position of each channel is labelled in the inset of (d). (e1–4) The maximum impact force of each pressing recorded in (c). (e-1) The impact force of each single pixel pressing from 1 to 9. (e-2) The impact force of 3 double pixel pressing: 1-2; 4-5 and 7-8. (e-3) The impact force of 3 double pixel pressing: 2-3; 5-6 and 8-9. (e-4) The impact force of 3 triple pixel pressing: 1-2-3; 4-5-6 and 7-8-9.

charge saturate or just break the hydrogel. For the sponge based device, the voltage and charge increase from 13.2 V and 10.4 nC to 25.9 nC, respectively, when the force increases from 15.5 N to 24.8 N. The effective force range for sponge based device is 13 N, which is almost 4 times higher than that of hydrogel based device, which is 3.2 N. In summary, compared with hydrogel based device, the sponge based device can provide higher output and larger force sensing range. To illustrate the force sensing applications, we demonstrated a local finger touching monitoring with WATENG. Fig. 3d displays a photograph of a 3 by 3 matrix pixel array where each pixel with a size of 2 cm by 2 cm was connected with the data acquisition system of 10 G Ω load resistance. When the top thick PDMS film was pressed by a finger with a representative force, corresponding output voltage signals of the 9 channels were observed, as illustrated in Fig. 3c. The number of each channel is indicated in Fig. 3d. The peak voltage of each pixel by pressing is recorded in Fig. 3e, representing the value of force. In the first step, single pixel was pressed following the sequence from 1 to 9. The peak value of each pixel is shown in Fig. 3e-1. In the second step, double pixels of the left and middle columns were pressed based on the sequence of 1-2, 4-5 and 7-8. The peak value of each pixel is shown in Fig. 3e-2. Then double pixels of the middle and right columns were pressed in sequence of 2-3, 5-6 and 8-9. Finally, three pixels were pressed together in sequence of 1-2-3; 4-5-6 and 7-8-9. The peak value of each pixel is shown in Fig. 3e-4. As shown in this demonstration, this array force sensor can be used to measure the finger pressing force and multiple pixels can be sensed simultaneously. A video demonstration of

the real-time force sensing can be found in [Supplementary information](#).

5. Selective stimulation of sciatic nerve

Selective stimulation of sciatic nerves may help paralyzed people to have balanced standing and efficient walking. A good control of various phases of gait requires specific ankle motions – dorsiflexion (DF) or plantar flexion (PF) –without the accompany of excessive foot inversion (FI) or eversion (FE) or toe flexion (TF) or extension (TE), meaning that in each phase of gait, only a specific group of nerves are selectively stimulated.

To evaluate the feasibility of the WATENG for neuroprosthetic application, we demonstrated selective stimulation of the sciatic nerve in rats using a flexible sling interface connected with a WATENG as a batteryless neurostimulator. The compound muscle action potentials (CMAPs) of tibialis anterior (TA) and gastrocnemius medialis (GM) muscles were recorded during the selective stimulation. The detailed rat preparation for *in vivo* test and physiological characterization were described in the [Supplementary information S4 and S5](#), respectively.

The several designs of neural interfaces were previously investigated for neural recording and selective stimulation of sciatic nerves such as split-ring, sling, and neural ribbon interfaces [9–11,48,49]. The split ring electrode performed the selective stimulation, although the number of electrodes was limited. The sling interface of six active and two bar electrodes coated with Pt-black enabled implantation around the nerve with less pressure and good

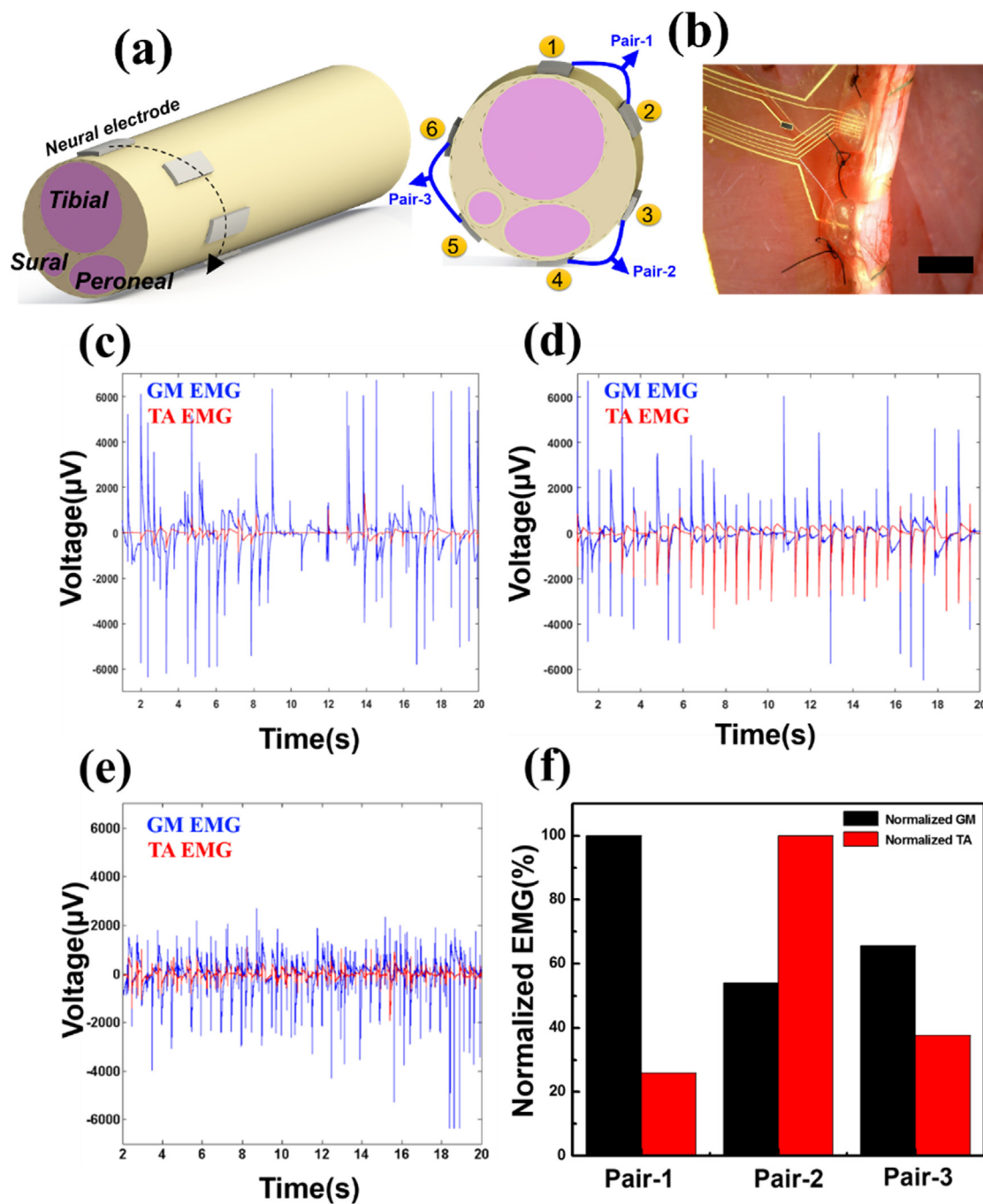


Fig. 4. (a) Schematic diagram of position and configuration of a sling interface implanted on a sciatic nerve, Pair-1 (active electrode 1 and 2), Pair-2 (active electrode 3 and 4), and Pair-3 (active electrode 5 and 6); (b) Optical image of the implanted sling interface on the sciatic nerve, the scale bar is 2 mm. The recorded compound muscle action potentials (CMAPs) of gastrocnemius medialis (GM) and tibialis anterior (TA) muscles stimulated by the configuration of (c) the pair-1; (d) the pair-2; (e) the pair-3; (f) The normalized EMG signals as a result of the stimulation by the 3 pairs of neural electrodes.

contact, to provide selective stimulation (Fig. 4a). The detailed electrochemical characterization of the sling interface was described in the [Supplementary information S6](#). Since the transverse configuration provided more effective stimulation of the muscles than longitudinal configuration [12], the six active electrodes in the central bridge of the sling interface connected to WATENG were used for this selective stimulation experiment. As shown in Fig. 4a, three pairs of active electrodes (Pair-1 with E1-E2, Pair-2 with E3-E4, and Pair-3 with E5-E6)

helically positioned on the sciatic nerve were used for the selective activation of the muscles via the WATENG, respectively. Fig. 4b shows a picture of the implanted sling interface on the sciatic nerve. The WATENG was applied with constant large forces which was roughly 19 N to each pair of the active electrode in order to compare the muscles activation as a result of different activation position. The amount of charge, which was between 10 and 20 nC, is reasonable to stimulate nerves though extra-neural approach based on the previous study [50].

Detailed force and charge output can be found in the [supplementary information S7](#). Muscle twitching was clearly observed for all the pairs while the stimulation. [Fig. 4c–e](#) shows the recorded CMAPs of GM (blue) and TA (red) muscles by the selective stimulation via the WATENG. For the pair-1, the recorded peak-to-peak amplitude of the CMAPs of GM and TA was 5000 μV and 570 μV , respectively. For the pair-2, the CMAPs of GM and TA was 2700 μV and 2100 μV , respectively. For the pair-3, the CMAPs of GM and TA was 3200 μV and 830 μV , respectively. The detailed information of the CMAP amplitudes is described in the [Supplementary information S8](#). The recorded peak-to-peak amplitudes of the CMAPs were then normalized to the highest amplitude in order to compare relative selectivity of the muscle activations caused by the stimulation of each pair as shown in [Fig. 4f](#). The pair-1 shows the maximum activation of the GM muscles and the minimum activation of the TA among the pairs while the pair-2 exhibits the completely opposite results. The pair-3 shows moderate activation of the both muscles compared with the other pairs. This indicates that the pair-1 is closer to a tibial nerve (which controls the GM muscle) and the pair-2 is near to a common peroneal (CP) nerve (which controls the TA muscles) as shown in [Fig. 4a](#). The results demonstrate that not only a selective stimulation using the WATENG connected with the neural interface can be achieved, but it also shows promising perspective as a battery-free neuromodulator in the future.

6. Force-controlled direction stimulation

During this *in vivo* experiment, two interesting phenomena were observed. The first observation was that no PF or DF were clearly observed by tapping the WATENG even with a large force higher than 30 N. This may be due to the fact that tibial nerve takes the largest cross-sectional area in sciatic nerve thus is more likely to be activated than the CP nerves. This result was observed from other studies as well [9,11,12,49]. Taking into account of the electrical energy required, we may be not able to modulate definite PF or DF unless a dedicated group of electrodes is positioned precisely on the CP nerve or the tibial nerve in the sciatic nerve, respectively. Therefore, neural electrodes and TENGs should be designed together depending on target nerves and the degree of muscle modulation. The second observation was that unique double-activation of the muscles occurs during pressing and releasing of the device with one tapping. This may be because the positive and negative peaks with different pulse widths stimulated the nerve differently.

To verify these assumptions and to demonstrate clear force-controlled modulation of the leg muscles in rats, we stimulated sciatic nerve branches (tibial nerve and CP nerve) using the WATENG connected with a pair of Pt/Ir wires. Approaching the small nerve branches will reduce the electrical energy required as well as enhance the selectivity of modulation of specific muscles. In particular, the CP nerve primarily innervates the TA muscle for ankle deflexors [50] while the tibial nerve mainly activates the GM muscle for ankle extensors [51]. In addition, the exposed Pt/Ir wires provide a higher contact area by smoothly wrapping around the branch nerves, allowing us to focus on demonstrating on force-controlled modulation of each muscle. [Fig. 5a](#) and [b](#) shows the pictures of implanted the Pt/Ir wires on the tibial nerve and the CP nerve, respectively. The stimulation was controlled by the force applied to the WATENG. We roughly classified the degree of stimulation into two groups: small force, which caused twitching but no complete muscle contraction, and large force, which lead to obvious muscle activation and contraction. The detailed force recordings and charge densities were described in the [Supplementary information S8](#). As expected, the GM muscle was activated more effectively than the TM muscle while the tibial nerve was stimulated, and clear PF was visible ([Fig. 5c](#)). On the other hand, we observed ankle DF ([Fig. 5d](#)) while the CP nerve stimulation showing the higher activation of the TA muscle than that of the GM muscle. When we applied the large force on the device, we clearly observed the double-activations in both nerves

([Figs. 5e](#) and [5f](#)). The first activation of the muscle was larger than the second activation.

We compared the time interval of the generated peaks from the device ([Figs. 5g](#) and [h](#)) and the time interval of the recorded stimulation artifacts from the first and the second activations of muscles. As indicated in [Fig. 5i](#) and [j](#), for tibial nerve stimulation, the time interval of the artifacts was consistent with the time interval of the two peaks as shown in [Fig. 5g](#). The same situation happened for CP nerve stimulation as shown in [Fig. 5k](#), [l](#), and [f](#). The interval times was approximately 60 ms in the both cases, indicating that the first sharp negative peak induces the first huge activation of the muscles and the following blunt positive peak causes the second small activation ([Fig. 5g](#) and [h](#)). However, when smaller force was applied, such double activations were not observed where the second current peak for small force was lower than 0.2 μA ([Fig. S4a](#) and [S4b](#)). The charge of the second peak generated by the small force may be less than the threshold charge for inducing muscle activation for both tibial nerve and CP nerve. These results demonstrate that the force-controlled modulation of the leg muscles in rats can be achieved using the WATENG connected with the neural interface by controlling the tapping force. A video demonstration of leg muscle modulation with different applied force can be found in [Supplementary information](#).

7. Waveform-dependent stimulation

From this *in vivo* experiment, we clearly observed contractions of the leg muscles. However, the stimulation currents generated by WATENGs were much lower than the conventional square pulse stimulation [14]. This interesting phenomenon has not been observed in any studies so far except the stimulation by TENGs. Even though the pulse widths were significantly higher than the conventional square wave stimulation, there was no observation of any kind of damage or degrading nerve function during the acute test. We assumed the shape of the generated peak by WATENGs caused this interesting phenomenon since there was a reported study that exponential waveform stimulated neuron more effectively than a square-wave pulse [14–16]. To prove this point, we investigated the efficiency of tibial nerve stimulation by biphasic square and exponential waveforms using external stimulation sources. The charge balanced biphasic square waveforms provide reliable and repetitive stimulation by reducing the possibility of electrode degradation and tissue damage [14]. Flexible neural clip (FNC) interfaces, which showed a good stimulation performance in the previous study, were used for this repetitive stimulation experiment ([Fig. 6a-i](#) and [a-ii](#)) [13]. In addition, we measured the contraction force by the leg muscle instead of recording CMAPs ([Fig. 6a-iii](#)). This is due to that the comparison of muscle force depending on the waveforms is a practical way to estimate efficient stimulation. In addition, the proportional relationship between EMG and muscle force was also demonstrated well in previous papers [52,53]. The positive and negative output current waveforms generated by WATENG were fitted by exponentially decreasing curves, respectively. The fitting exponential waveforms were generated by the external source for stimulation in the tests ([Fig. 6b](#) and [c](#)).

For a clear comparison of the measured forces by different waveforms, the exponential waveforms were rescaled with amplitude and duration to activate a clear muscle contraction and generate a stable force large enough to be recorded by our system. In addition, the square waveforms that generate the force at the same range were applied for the comparison. The testing results are shown in [Fig. 6d](#). As for the square waveform, we changed the current from 500 μA to 1300 μA and the duration of the single phase from 500 μs to 1200 μs . When the current was lower than 500 μA , there was either no clear stimulation or only slightly twitching only when the current was higher than 500 μA , clear and stable force was recorded. For the current of 500 μA , 700 μA and 1000 μA , the force kept constant when the pulse width was changed. Only for the current of 1300 μA , the force increased with the

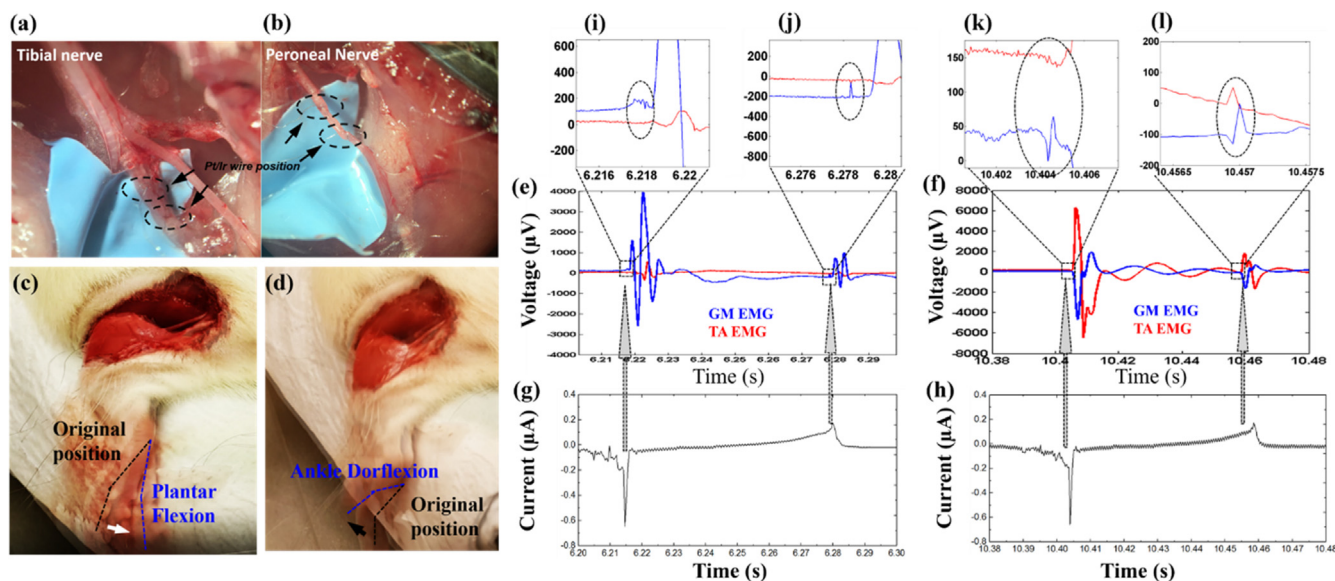


Fig. 5. The result of force-controlled modulation of leg muscles in rats. (a)(b) Optical images of the tibial nerve and the common peroneal (CP) nerves with the implantation of a pair of Pt/Ir wires, respectively. (c) The plantar flexion induced by the tibial nerve stimulation with the large tapping force on the triboelectric based force sensing array. (d) The ankle dorsiflexion induced by the CP nerve stimulation with the large tapping force on the triboelectric based force sensing array. The recorded compound muscle action potentials (CMAPs) from (e) the tibial nerve stimulated and (f) the CP nerve by the current signal (g) and (h) when large force was applied, respectively. The artifact generated by negative peak (i) and positive peak (j) of the current signal in (g) for tibial nerve; the artifact generated by negative peak (k) and positive peak (l) of the current signal in (h) for peroneal nerve.

pulse width. As for the exponential waveform, the force was recoded at the 200 μA current and increased linearly with the pulse width. There was no obvious difference between the positive and negative exponential waveform in this study. At the pulse width of 500 μs , the exponential waveform generated a force of 0.045 N, which was comparable with the force of 1000 μA square waveform at the same pulse width. Then, with a larger pulse width, the force generated by the exponential waveform was always higher than that of square waveform, except for the 1300 μA . This result clearly shows that the exponential waveform induces higher force even with a much lower current.

Based on the previous research, it is widely believed that the threshold charge is important to determine the minimum stimulation amplitude required to excite neurons and nerves [14]. According to this view point, the Fig. 6d is replotted as Fig. 6e in terms of charge. The charge of each waveform is calculated using the current amplitude and the pulse width. The curves of the exponential wave are shown in the inset since their charge quantity is much lower than that of the square waveforms. The exponential waveform only provides very minimum charge but can achieve relatively large force. Meanwhile, the force generated by the square wave does not increase with charge unless the current is higher than a threshold, which is 1300 μA in our test.

Our test confirms that the special current waveform of the WATENG can be more effective than the square waveform for nerve stimulation. This exponentially decreasing waveform requires much less current and charge to generate the same force compared with the square waveform stimulation. This result reveals that other than the quantity of the charge, the shape of the current waveform is also a major factor to determine the stimulation result. Further investigation of the detailed mechanism is worthy to be explored in the future.

One interesting phenomenon was observed that the force increases monotonically and linearly with input charge of the exponential wave while the relation between the force and charge of the square wave is not very clear. The similar phenomenon was also observed in the test of nerve branches stimulated by WATENG, a higher pressing force to generate more charge, higher output voltage and current, then finally result in a stronger muscle contraction. It indicates a good linear control

capability of WATENG stimulation. Since currently it is not clear that which parameter, either voltage, current or charge, truly affects the stimulation result, a detailed characterization of all these three parameters are conducted.

8. Concluding remarks

A novel water/air-hybrid triboelectric nanogenerator (WATENG) was developed in this study for peripheral nerve stimulation. The suspended dielectric thin film significantly amplified the output voltage of the liquid involved TENGs from mV level up to tens of volt. With the sponge filled with water, the drawbacks of the conventional liquid involved TENGs, which utilize multiple phases of water droplet, water evaporation and fixation, could be improved. As an alternative to hydrogel, sponge based device was more robust, enabling a four times higher force sensing range. Selective stimulation of a sciatic nerve in rats via flexible sling interfaces induced selective activation of the leg muscles monitored by EMG signals. In addition, the output charge amplified by the suspended dielectric thin film was able to induce plantar flexion (PF) and ankle dorsiflexion (DF) via tibial and common peroneal (CP) nerve branches. Meanwhile the amplitude of the muscle activation was modulated by controlling the pressing force. A detailed comparison between the biphasic square waveform and exponentially decreasing waveform were conducted to verify the high effectiveness of WATENG for nerve stimulation using flexible neural clip interfaces. The result demonstrated that the special waveform of the WATENG output current is more efficient for nerve stimulation with better linear control. By combining WATENG with neural interfaces, battery-free and wearable neuromodulator would be realized in the future. Furthermore, recent studies of implantable nanogenerators demonstrate the capability of implanting on muscles or organs for harvesting energy or monitoring its movement inside body [21,29,32,54–58]. Considering anatomical shapes or physiological motions of muscle or organs, well designed TENG could be implanted with implantable neural interfaces to realize battery-free neuromodulator in the future.

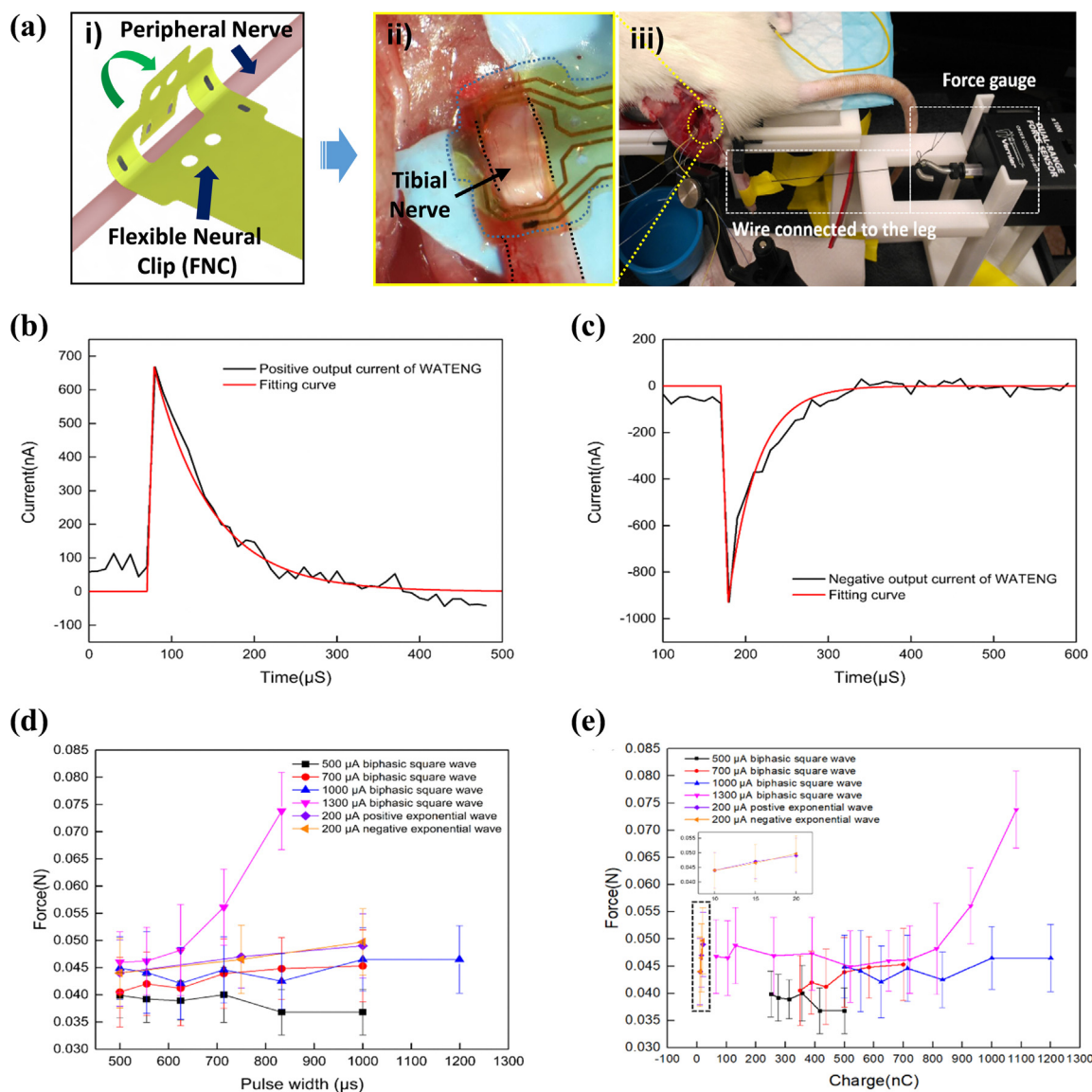


Fig. 6. The result of the efficiency of nerve stimulation dependin on the waveforms. (a) Experimental setup; i) The steps involved in implanting flexible neural clip (FNC), ii) a picture of implanted FNC on a tibial nerve, and iii) a picture of experimental setup for the force-measurement. (b) A typical positive current output of the WATENG and the fitting curve. (c) A typical negative current output of the WATENG and the fitting curve. (d) The force generated by nerve stimulation with biphasic square waveform and exponential waveform of different current and pulse width. (e) The replotted data of the force as a result of the calculated charge.

Acknowledgements

This work was supported by grants from the National Research Foundation (NRF) CRP project ‘Self-Powered Body Sensor Network for Disease Management and Prevention Oriented Healthcare’ (R-263-000-A27-281), National Research Foundation (NRF) CRP project ‘Peripheral Nerve Prostheses: A Paradigm Shift in Restoring Dexterous Limb Function’ (R-719-000-001-281), National Research Foundation (NRF) CRP project ‘Energy Harvesting Solutions for Biosensors’ (R-263-000-A27-281), Ministry of Education (MOE) Faculty Research Committee (FRC) Grant (R-263-000-B56-112) ‘Thermoelectric Power Generator (TEG) Based Self-Powered ECG Plaster – System Integration (Part 3)’, Hybrid Integrated Flexible Electronic Systems (HIFES) ‘Hybrid Integration of Flexible Power Source and Pressure Sensors’, Seed Funding-2017-01 (R-263-501-012-133), National Natural Science Foundation of China under Grant no. 61474078 at NUS (Suzhou) Research Institute, Suzhou, China.

Appendix A. Supporting information

Supplementary data associated with this article can be found in the online version at <http://dx.doi.org/10.1016/j.nanoen.2018.04.004>.

References

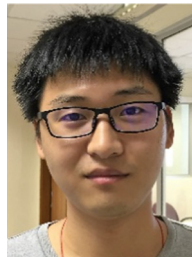
- [1] D. Farina, O. Aszmann, *Sci. Transl. Med.* 6 (2014) 257ps212.
- [2] S. Raspopovic, M. Capogrosso, F.M. Petrini, M. Bonizzato, J. Rigosa, G. Di Pino, J. Carpaneto, M. Controzzi, T. Boretius, E. Fernandez, G. Granata, C.M. Oddo, L. Citi, A.L. Ciancio, C. Cipriani, M.C. Carrozza, W. Jensen, E. Guglielmelli, T. Stieglitz, P.M. Rossini, S. Micera, *Sci. Transl. Med.* 6 (2014) 222ra219.
- [3] D.W. Tan, M.A. Schiefer, M.W. Keith, J.R. Anderson, J. Tyler, D.J. Tyler, *Sci. Transl. Med.* 6 (2014) 257ra138.
- [4] K. Famm, B. Litt, K.J. Tracey, E.S. Boyden, M. Slaoui, *Nature* 496 (2013) 159–161.
- [5] S. Reardon, *Nature* 511 (2014) 18.
- [6] I. Adameyko, *Science* 354 (2016) 833–834.
- [7] G. Di Pino, L. Denaro, G. Vadala, A. Marinuzzi, M. Tombini, F. Ferreri, R. Papalia, D. Accoto, E. Guglielmelli, V. Di Lazzaro, V. Denaro, *J. Surg. Res.* 188 (2014) 77–87.
- [8] S. Lee, S.C. Yen, S. Sheshadri, I. Delgado-Martinez, N. Xue, Z. Xiang, N.V. Thakor, C. Lee, *IEEE Trans. Biomed. Eng.* 63 (2016) 581–587.
- [9] Z. Xiang, S. Sheshadri, S.H. Lee, J. Wang, N. Xue, N.V. Thakor, S.C. Yen, C. Lee, *Adv.*

- Sci. 3 (2016) 1500386.
- [10] Z. Xiang, S.C. Yen, S. Sheshadri, J. Wang, S. Lee, Y.H. Liu, L.D. Liao, N.V. Thakor, C. Lee, *Adv. Mater.* 28 (2016) 4472–4479.
- [11] S. Lee, S. Sheshadri, Z. Xiang, I. Delgado-Martinez, N. Xue, T. Sun, N.V. Thakor, S.-C. Yen, C. Lee, *Sens. Actuators B: Chem.* 242 (2017) 1165–1170.
- [12] S. Lee, H. Wang, Q. Shi, L. Dhakar, J. Wang, N.V. Thakor, S.-C. Yen, C. Lee, *Nano Energy* 33 (2017) 1–11.
- [13] S. Lee, W.Y.X. Peh, J. Wang, F. Yang, J.S. Ho, N.V. Thakor, S.C. Yen, C. Lee, *Adv. Sci.* 4 (2017) 1700149.
- [14] D.T. Brocker, W.M. Grill, *Handb. Clin. Neurol.* 116 (2013) 3–18.
- [15] A. Wongsarnpigoon, W.M. Grill, *IEEE EMBS* (2009) 634–637.
- [16] M. Yip, P. Bowers, V. Noel, A. Chandrakasan, K.M. Stankovic, *Sci. Rep.* 7 (2017) 13582.
- [17] G.T. Hwang, Y. Kim, J.H. Lee, S. Oh, C.K. Jeong, D.Y. Park, J. Ryu, H. Kwon, S.G. Lee, B. Joung, D. Kim, K.J. Lee, *Energy Environ. Sci.* 8 (2015) 2677–2684.
- [18] H. Zhang, X.S. Zhang, X. Cheng, Y. Liu, M. Han, X. Xue, S. Wang, F. Yang, S. A. S. H. Zhang, Z. Xu, *Nano Energy* 12 (2015) 296–304.
- [19] X. Cheng, X. Xue, Y. Ma, M. Han, W. Zhang, Z. Xu, H. Zhang, H. Zhang, *Nano Energy* 22 (2016) 453–460.
- [20] C.K. Jeong, S.B. Cho, J.H. Han, D.Y. Park, S. Yang, K.I. Park, J. Ryu, H. Sohn, Y.C. Chung, K.J. Lee, *Nano Res.* (2016).
- [21] A. Wang, Z. Liu, M. Hu, C. Wang, X. Zhang, B. Shi, Y. Fan, Y. Cui, Z. Li, K. Ren, *Nano Energy* 43 (2018) 63–71.
- [22] P. Bai, G. Zhu, Z.H. Lin, Q. Jing, J. Chen, G. Zhang, J. Ma, Z.L. Wang, *ACS Nano* 7 (2013) 3713–3719.
- [23] X.S. Zhang, M.D. Han, R.X. Wang, F.Y. Zhu, Z.H. Li, W. Wang, H.X. Zhang, *Nano Lett.* 13 (2013) 1168–1172.
- [24] B. Meng, W. Tang, X.S. Zhang, M. Han, W. Liu, H. Zhang, *Nano Energy* 2 (2013) 1101–1106.
- [25] Q. Zheng, B. Shi, F. Fan, X. Wang, L. Yan, W. Yuan, S. Wang, H. Liu, Z. Li, Z.L. Wang, *Adv. Mater.* 26 (2014) 5851–5856.
- [26] X.H. Li, C.B. Han, L.M. Zhang, Z.L. Wang, *Nano Res.* 8 (2015) 3197–3204.
- [27] J. Chun, B.U. Ye, J.W. Lee, D. Choi, C.Y. Kang, S.W. Kim, Z.L. Wang, J.M. Baik, *Nat. Commun.* 7 (2016) 12985.
- [28] H. Wang, Z. Xiang, P. Giorgia, X. Mu, Y. Yang, Z.L. Wang, C. Lee, *Nano Energy* 23 (2016) 80–88.
- [29] Q. Zheng, H. Zhang, B. Shi, X. Xue, Z. Liu, Y. Jin, Y. Ma, Y. Zou, X. Wang, Z. An, W. Tang, W. Zhang, F. Yang, Y. Liu, X. Lang, Z. Xu, Z. Li, Z.L. Wang, *ACS Nano* 10 (2016) 6510–6518.
- [30] X.-S. Zhang, M. Su, J. Brugger, B. Kim, *Nano Energy* 33 (2017) 393–401.
- [31] J. Sun, W. Li, G. Liu, W. Li, M. Chen, J. Phys. Chem. C. 119 (2015) 9061–9068.
- [32] Q. Zheng, Y. Zou, Y. Zhang, Z. Liu, B. Shi, X. Wang, Y. Jin, H. Ouyang, Z. Li, Z.L. Wang, *Sci. Adv.* 2 (2016) e1501478.
- [33] X.S. Zhang, M.D. Han, R.X. Wang, B. Meng, F.Y. Zhu, X.M. Sun, W. Hu, W. Wang, Z.H. Li, H.X. Zhang, *Nano Energy* 4 (2014) 123–131.
- [34] W. Kong, L. Cheng, X. He, Z. Xu, X. Ma, Y. He, L. Lu, X. Zhang, Y. Deng, *Microfluid. Nanofluidics* 18 (2014) 1299–1307.
- [35] S.-H. Kwon, J. Park, W.K. Kim, Y. Yang, E. Lee, C.J. Han, S.Y. Park, J. Lee, Y.S. Kim, *Energy Environ. Sci.* 7 (2014) 3279–3283.
- [36] Z.H. Lin, G. Cheng, S. Lee, K.C. Pradel, Z.L. Wang, *Adv. Mater.* 26 (2014) 4690–4696.
- [37] L.E. Helseth, X.D. Guo, *Smart Mater. Struct.* 25 (2016) 045007.
- [38] S.-B. Jeon, M.-L. Seol, D. Kim, S.-J. Park, Y.-K. Choi, *Adv. Electron. Mater.* 2 (2016) 1600006.
- [39] X. Wu, G. Li, D.-W. Lee, *Appl. Energy* 173 (2016) 103–110.
- [40] W. Xu, L.-B. Huang, M.-C. Wong, L. Chen, G. Bai, J. Hao, *Adv. Energy Mater.* 7 (2017) 1601529.
- [41] J.K. Moon, J. Jeong, D. Lee, H.K. Pak, *Nat. Commun.* 4 (2013) 1487.
- [42] D. Kim, K.S. Yun, *J. Phys.: Confer. Ser.* 660 (2015) 012108.
- [43] L.E. Helseth, *J. Electrostat.* 81 (2016) 64–70.
- [44] F.R. Fan, Z.Q. Tian, Z.L. Wang, *Nano Energy* 1 (2012) 328–334.
- [45] Y. Zi, S. Niu, J. Wang, Z. Wen, W. Tang, Z.L. Wang, *Nat. Commun.* 6 (2015) 8376.
- [46] H. Guo, Q. Leng, X. He, M. Wang, J. Chen, C. Hu, Y. Xi, *Adv. Energy Mater.* 5 (2015) 1400790.
- [47] J. Zhong, H. Zhu, Q. Zhong, J. Dai, W. Li, S.H. Jang, Y. Yao, D. Henderson, Q. Hu, L. Hu, J. Zhou, *ACS Nano* 9 (2015) 7399–7406.
- [48] N. Xue, T. Sun, W.M. Tsang, I. Delgado-Martinez, S.-H. Lee, S. Sheshadri, Z. Xiang, S. Merugu, Y. Gu, S.-C. Yen, N.V. Thakor, *Sens. Actuators B: Chem.* 210 (2015) 640–648.
- [49] S. Lee, S.C. Yen, L.D. Liao, G.G.L. Gammad, N.V. Thakor, C. Lee, *Micro Electro Mechanical Systems (MEMS)*, 2016 IEEE 29th International Conference on, 2016, pp. 375–378.
- [50] J.H. Burridge, D.L. McLellan, *J. Neurol. Neurosurg. Psychiatry* 69 (2000) 353–361.
- [51] J. Badia, T. Boretius, D. Andreu, C. Azevedo-Coste, T. Stieglitz, X. Navarro, *J. Neural Eng.* 8 (2011) 036023.
- [52] P.J. Whelan, *Methods* 30 (2003) 127–141.
- [53] H.U. Kuriki, F.M. Azevedo, L.S.O. Takahashi, E.M. Mello, R.F.N. Filho, N. Alves, The relationship between electromyography and muscle force, EMG methods for evaluating muscle and nerve function, INTECH, 2012, pp. 31–54.
- [54] Z. Li, G. Zhu, R. Yang, A.C. Wang, Z.L. Wang, *Adv. Mater.* 22 (2010) 2534–2537.
- [55] M.A. Parvez Mahmud, N. Huda, S.H. Farjana, M. Asadnia, C. Lang, *Adv. Energy Mater.* 8 (2018) 1701210.
- [56] H. Ouyang, J. Tian, G. Sun, Y. Zou, Z. Liu, H. Li, L. Zhao, B. Shi, Y. Fan, Y. Fan, Z.L. Wang, Z. Li, *Adv. Mater.* 29 (2017) 1703456.
- [57] H. Feng, C. Zhao, P. Tan, R. Liu, X. Chen, Z. Li, *Adv. Healthc. Mater.* 0 (2018) 1701298.

- [58] X.S. Zhang, M. Han, B. Kim, J.F. Bao, J. Brugger, H. Zhang, *Nano Energy* 47 (2018) 410–426.



Sanghoon Lee received the B.S. degree at the Department of Electronic Material Engineering in Kwangwoon Univ., Seoul, Korea in 2009 as well as his M.Eng. and Ph.D. degrees at the Department of Electrical and Computer Engineering (ECE), National University of Singapore (NUS), Singapore in 2013 and 2017, respectively. His Ph.D. thesis focused on the design and development of flexible neural interface for recording and stimulation of peripheral and visceral nerves. He is currently working as a research fellow at Singapore Institute for Neurotechnology (SINAPSE), NUS. He is working on the development of advance neural interface for bioelectronic medicine and neural prostheses.



Hao Wang received Hao Wang received the B.Eng. degree from the School of Optoelectronic Information, University of Electronic Science and Technology of China, in 2010. He is currently pursuing the M.Eng. degree with the Department of Electrical and Computer Engineering. He is also a Research Engineer of Electrical and Computer Engineering with the National University of Singapore. His research interests are focused on nanoneedle devices for transdermal drug delivery.



Jiahui Wang is currently a Ph.D. candidate in Department of Electrical & Computer Engineering, National University of Singapore. She received her Bachelor's degree in Department of Microelectronics, Fudan University in 2014. She is mainly interested in implantable neural interfaces, biocompatible sensors and energy applications.



Qiongfeng Shi received his B.Eng. degree from Department of Electronic Engineering and Information Science at University of Science and Technology of China (USTC) in 2012. He is currently pursuing his Ph.D. degree in the Department of Electrical and Computer Engineering, National University of Singapore (NUS) under the NUS research scholarship. His research interests are mainly focused on energy harvesters and self-powered sensors.



Shih-Cheng Yen received his B.S.E. and M.S.E. in 1993, and his Ph.D. in 1998, all from the Department of Bioengineering at the University of Pennsylvania. For his Ph.D., he worked on neural network models of the primary visual cortex. He was a Research Assistant Professor at Montana State University. He is currently an Assistant Professor in the Department of Electrical and Computer Engineering at the National University of Singapore (NUS), and the Deputy Director of the Singapore Institute for Neurotechnology (SINAPSE) at NUS. His research interests are in neural coding and neuroprosthetics.



Nitish V. Thakor is the Director the Singapore Institute for Neurotechnology (SINAPSE) at the National University of Singapore and the Professor of Electrical and Computer Engineering and Biomedical Engineering. Previously he was the Professor of Biomedical Engineering at Johns Hopkins University. Prof. Thakor's technical expertise is in the field of Neuroengineering, where he has pioneered many technologies for brain monitoring to prosthetic arms and neuroprosthesis. He is currently the Editor in Chief of Medical and Biological Engineering and Computing, and was the Editor in Chief of IEEE TNSRE from 2005 to 2011.



Chengkuo Lee is the director of Center for Intelligent Sensors and MEMS at National University of Singapore. He received M.Sc. in Department of Materials Science & Engineer, National Tsing Hua University, Taiwan in 1991, M.Sc. in Department of Industrial & System Engineering, the State University of New Jersey, Rutgers, USA in 1993, and Ph.D. in Department of Precision Engineering, University of Tokyo, Japan in 1996. He is general chair of IEEE NEMS 2018. He has published more than 250 peer-reviewed journal articles. His research interests include energy harvesting, biomedical devices, flexible electronics, photonics, MEMS and NEMS.